National Aeronautics and Space Administration

Jet Propulsion Laboratory
California Institute of Technology
Pasadena, California

The Madden-Julian Oscillation and Atmospheric Composition

Baijun Tian[1], Duane E. Waliser[1], and Yuk L. Yung[2]

1. Jet Propulsion Laboratory, California Institute of Technology, Pasadena, CA.
2. Division of Geological and Planetary Sciences, California Institute of Technology, Pasadena, CA.

I. Introduction

➢The **Madden-Julian Oscillation (MJO)** (aka Intraseasonal Oscillation) [*Madden and Julian*, 1971; 1994] is the dominant component of intraseasonal variability in the tropical atmosphere. It is characterized by slow (~5 m/s) eastward-propagating, large-scale oscillations in tropical deep convection and the baroclinic wind field, especially over the warmest tropical waters in the equatorial Indian and western Pacific Oceans [e.g., *Hendon and Salby*, 1994]. Such characteristics tend to be most strongly exhibited during boreal winter (Nov-Apr), when the Indo-Pacific warm pool is centered near the equator. *Lau and Waliser* [2005] and *Zhang* [2005] provide a comprehensive review of the MJO and related issues.

➢The MJO has been shown to have important influences on other parts of **the physical weather and climate system**, e.g., diurnal cycle, Asian and Australian monsoon onsets and breaks, tropical hurricanes, extreme precipitation events, extra-tropical circulation and its weather patterns, El Niño-Southern Oscillation and ocean climate [*Lau and Waliser*, 2005]. The interactions of the MJO and other parts of the physical weather and climate system, in many cases, have been well documented, and in a few cases, well understood. **However, the impact of the MJO on atmospheric composition has yet to be well documented.** In this study, we explore the influence of the MJO on **atmospheric composition, specifically ozone and aerosols**, using satellite remotely-sensed ozone and aerosol products.

II. Ozone and Aerosol Data

➢**Total Ozone Mapping Spectrometer (TOMS)/Solar Backscatter Ultraviolet (SBUV) Merged Ozone Dataset (MOD):**
V8, 5°x10° lat-long, daily, from Jan 1980 to Jun 2006. Merged from 6 satellite instruments: Nimbus-7 and Earth Probe TOMS, Nimbus-7 SBUV, NOAA 9, 11, and 16 SBUV2s. Ref: *Stolarski and Frith* [2006].

➢**Atmospheric Infrared Sounder (AIRS) Total Ozone:**
L3, 1° x 1°, twice daily, from Sep 2002 to Jul 2006. NASA Aqua Satellite. Ref: *Chahine et al*. [2006].

➢**Nimbus-7 TOMS Aerosol Index (AI):**
L3, V8, 1°x1.25° lat-long, daily, from Jan 1980 to Dec 1992. AI, calculated from UV radiances at 0.331 and 0.360 µm, can detect the elevated UV-absorbing aerosols over both ocean and land, above clouds [*Herman et al.*, 1997].

➢**Moderate Resolution Imaging Spectroradiometer (MODIS) Aerosol Optical Thickness (AOT):**
L3, V4, MOD08, 1° x 1°, 0.55µm, daily, from Feb 2000 to Dec 2005. Derived from clear-sky radiances in 6 bands (0.55, 0.66, 0.87, 1.24, 1.64, and 2.13 µm) over ocean [*Tanre et al.* 1997; *Levy et al.* 2003; *Remer et al.* 2005] and in three bands (0.47, 0.66, and 2.13 µm) over land [*Kaufman et al.* 1997; *Remer et al.* 2005].

➢**Global Aerosol Climatology Project (GACP)/Advanced Very High Resolution Radiometer (AVHRR) AOT:**
1° x 1°, 0.55 µm, daily, ocean only, from Jan 1982 to Jun 2005. Derived from clear-sky calibrated AVHRR channel 1 (0.63 µm) and 2 (0.85 µm) radiances contained in the ISCCP DX data set [*Mishchenko et al.*, 1999; *Geogdzhayev et al.*, 2002; *Mishchenko and Geogdzhayev*, 2007].

➢**Aerosol Robotic Network (AERONET) AOT:**
L2.0 (cloud-screened and quality-assured), V2.0, daily AOT at 0.55 µm. Kaashidoo (73.5E, 4.9N), from Feb 1998 to Jul 2000. Nauru (167E, 0.5S), from Jun 1999 to Jun 2006 [*Holben et al.*, 1998; 2001].

➢**NCEP/NCAR Reanalysis Geopotential Height and Stream Function:**
2.5° x 2.0°, daily, from Jan 1979 to Dec 2006. Ref: *Kalnay et al.* [1996].

➢**NOAA Climate Prediction Center (CPC) Merged Analysis of Precipitation (CMAP) Rainfall**:
2.5° x 2.5°, pentad (5-day), from Jan 1979 to May 2006. Ref: *Xie and Arkin* [1997].

III. MJO Analysis Method and Event Selection

➢ Bin the data into 5-day average (pentad) values.
➢ Remove the annual cycle.
➢ Band-pass filter (30-90 day) the data.
➢ Identify MJO events using Extended EOF analysis using +/- 5 pentad lags (11 pentads, 55 days) of rainfall anomaly.
➢ Composite selected MJO events. Refs: *Waliser et al.* [2003] and *Tian et al.* [2006].

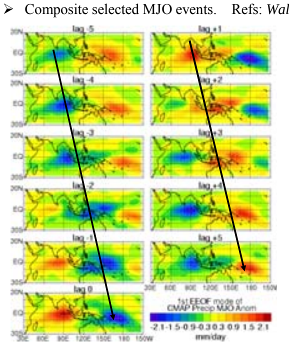

Figure 1: Spatial–temporal pattern for the first EEOF mode of filtered (30-90 days) boreal winter (Nov–Apr) CMAP rainfall anomaly in the region 30°S–30°N and 30°E–150°W. The unit for the lag is pentad.

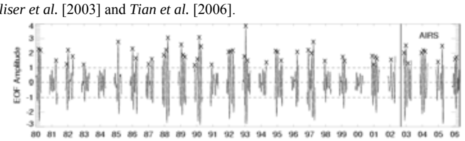

Figure 2: The dates (indicated by x) of selected MJO events for ***ozone*** study: MOD (55, Jan 1980 to Jun 2006) and AIRS (10, Sep 2002 to Jul 2006) periods, based on the amplitude pentad time series for the first EEOF mode of CMAP rainfall anomaly. Three dashed lines show the EEOF amplitude of ±1 and 0. The solid line indicates the start of the AIRS data record (09/2002).

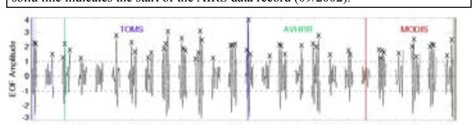

Figure 3: The dates (indicated by x) of selected MJO events for ***aerosol*** study: TOMS (26, Jan 1980 to Dec 1992), MODIS (13, Feb 2000 to Jun 2005), and AVHRR (48, Jan 1982 to May 2005) periods, based on the amplitude pentad time series for the first EEOF mode of CMAP rainfall anomaly. The solid colored lines indicate the start and end of each data record (blue for TOMS, red for MODIS, and green for AVHRR).

IV. Main Results for Ozone

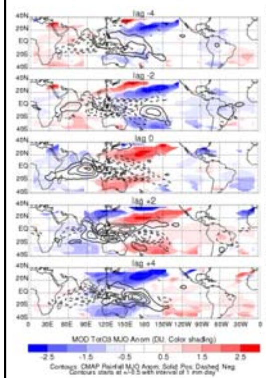

Figure 4: Composite MOD total O3 (color shading) and CMAP rainfall (black contours) MJO anomalies. Only the total O3 anomalies with above 95% confidence limit are shown.

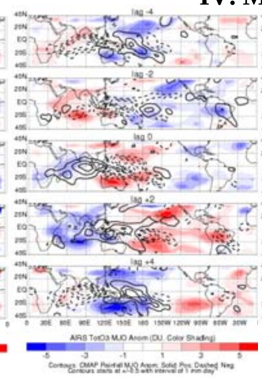

Figure 5: As Fig 4 but for AIRS total O3 MJO anomalies with different color scale.

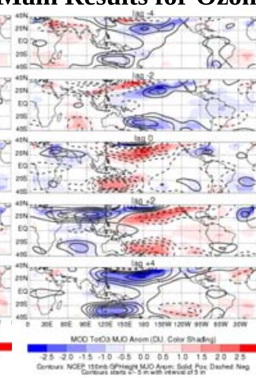

Figure 6: Composite MOD total O3 (color shading) and NCEP 150-hPa geopotential height (black contours) MJO anomalies.

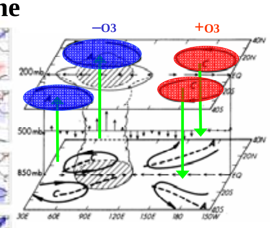

Figure 7: Schematic of the total ozone anomalies and their connection to the MJO. The cloud symbol indicates the equatorial MJO convective center. Black arrows represent anomalous winds at 850 and 200 hPa and the vertical motions at 500 hPa. ''A'' and ''C'' mark the anticyclonic and cyclonic circulation centers, respectively. Dashed lines indicate troughs and ridges. Green arrows denote the vertical movement of the subtropical tropopause. Blue ovals represent negative ozone anomalies, while red ovals denote positive ozone anomalies. Adapted from *Rui and Wang* [1990].

➢The MJO-driven variations of tropical total ozone are large (~±2.5 DU) and comparable to those in annual and interannual time scales (**Figs 4 & 5**).
➢Significant ozone variation are mainly evident in the subtropics over the Pacific and eastern hemisphere, while equatorial ozone variations are small (**Figs 4 & 5**).
➢ Subtropical ozone variations are related to the subtropical cyclone/anticyclone generated by equatorial MJO convection which produces vertical movement of the subtropical tropopause (**Figs. 6 & 7**). This implies the subtropical ozone variations are mainly from stratospheric contribution.
➢AIRS and MOD ozone variations have similar gross spatial and temporal patterns, but detailed differences exist, especially in magnitude (**Fig. 5**).

V. Main Results for Aerosols

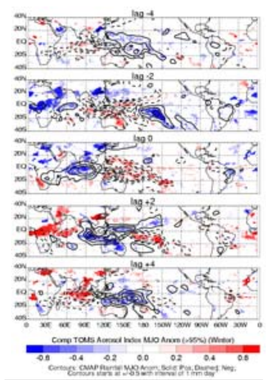

Figure 8: Composite maps of TOMS AI anomalies (color shading) above 95% confidence level and CMAP rainfall anomalies (contours).

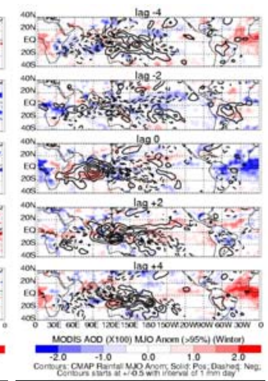

Figure 9: Composite maps of MODIS AOT anomalies (color shading) above 95% confidence level and CMAP rainfall anomalies (contours).

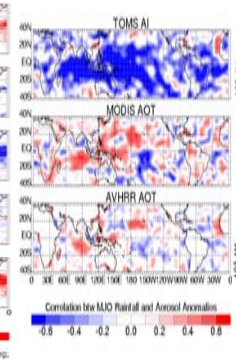

Figure 10: The zero-lag correlation between the composite anomalies of CMAP rainfall and TOMS AI, MODIS AOT, and AVHRR AOT.

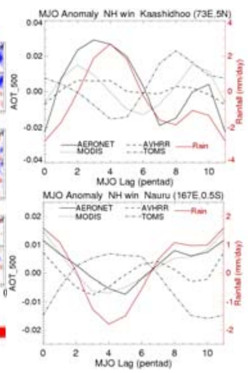

Figure 11: AERONET AOT, TOMS AI, MODIS AOT, AVHRR AOT and CMAP rainfall composite MJO anomalies at Kaashidoo and Nauru.

➢Large intraseasonal aerosol variations are found mainly over the equatorial Indian Ocean and western Pacific Ocean, where MJO convection is strongest, as well as tropical Africa and the Atlantic Ocean, where MJO convection is weak but the background aerosol loading is high (**Figs 8 & 9**).
➢There is a strong negative correlation between TOMS AI and rainfall anomalies but a weaker and less coherent positive correlation between MODIS/AVHRR AOT and rainfall anomalies (**Figs 8, 9 & 10**). The later is more consistent with AERONET data (**Fig 11**).
➢Aerosol humidification effect, wet deposition, surface wind speed, phytoplankton, different sensor sensitivities (absorbing versus non-absorbing, upper- versus lower-level aerosols), sampling issue, and cloud contamination may contribute to the observed aerosol-rainfall relationship. However, a clear causal explanation still remains elusive.

VI. Key Summary Point

Using satellite remotely-sensed ozone and aerosol products, we have found that the MJO can induce systematic and significant variations in atmospheric composition, such as ozone and aerosols, through its either convective (aerosols) or dynamic effect (ozone).

VII. Questions Raised

➢Can chemistry-transport models replicate these ozone and aerosol features given MJO-related forcing?
➢Do the models and/or ozonesondes support the notion that tropospheric variations play a little role in the subtropical ozone variations?
➢In the equatorial regions, what are the dynamic versus chemical and stratospheric versus tropospheric contributions to the ozone variations?
➢Are these aerosol-rainfall relationships physical, or is one or more of them a result of the aerosol sampling and/or retrieval artifacts?
➢Why is the correlation between TOMS AI and rainfall anomalies negative but positive between MODIS/AVHRR AOT and rainfall anomalies?
➢What is the relative contribution of aerosol humidification effect, wet deposition, surface wind speed, phytoplankton, sampling issue, and cloud contamination in the observed aerosol-rainfall relationships? Can models help us to understand these questions?

Acknowledgement:
We thank T. Tyranowski, L. Kuai, E. J. Fetzer, F. W. Irion, R. A. Kahn, Q. Li, I. V. Geogdzhayev, M. I. Mishchenko, and O. Torres for help. This work was supported by the Research and Technology Development program, Human Resources Development fund, and AIRS project at JPL as well as NASA Modeling, Analysis and Prediction program. The research at JPL, Caltech was performed under contracts with the NASA.

References:
Tian, B. J., D. E. Waliser, R. A. Kahn, Q. B. Li, **Y. L. Yung**, T. Tyranowski, I. V. Geogdzhayev, M. I. Mishchenko, and O. Torres (2007), Does the Madden-Julian oscillation influence aerosol variability? *J. Geophys. Res.*, submitted.
Tian, B. J., Y. L. Yung, D. E. Waliser, T. Tyranowski, L. Kuai, E. J. Fetzer, and F. W. Irion (2007), Intraseasonal variations of the tropical total ozone and their connection to the Madden-Julian oscillation, *Geophys. Res. Lett.*, *34*, L08704, doi:10.1029/2007GL029451.
Tian, B. J., D. E. Waliser, E. J. Fetzer, B. H. Lambrigtsen, **Y. L. Yung**, and B. Wang (2006), Vertical moist thermodynamic structure and spatial-temporal evolution of the MJO in AIRS observations, *J. Atmos. Sci.*, *63*, 2462-2485.

Dr. Baijun Tian, Jet Propulsion Laboratory, California Institute of Technology, 4800 Oak Grove Dr., M/S. 183-501, Pasadena CA 91109. Email: baijun.tian@jpl.nasa.gov